

## SEMI-TRANSPARENT AMORPHOUS SILICON SOLAR CELLS ON INEXPENSIVE PLASTIC SUBSTRATES

I. Matulionis<sup>a,b</sup>, Jian Hu<sup>a</sup>, A. Stavrides<sup>a</sup>, N. Call<sup>a,b</sup>, A. Kunrath<sup>a</sup>, Arun Madan<sup>a,b</sup>

a) MVSystems, Inc., 500 Corporate Circle, Suite L, Golden, CO, USA 80401

b) Department of Metallurgical and Materials Engineering, Colorado School of Mines, Golden, CO 80401

### ABSTRACT

We report a monolithic series connected semi-transparent (transmission > 40%) amorphous Silicon (*a*-Si:H) solar cell panel (substrate area 30cm × 40cm), which has an i-layer thickness <2000Å and an active area efficiency,  $\eta \sim 3\%$ . We also report on all laser scribed, series connected mini-modules with an aperture area  $\eta > 3\%$  constructed on inexpensive plastic substrates.

### INTRODUCTION

Crystalline Si/poly-crystalline Si solar cells presently dominate the photovoltaic market. Due to a low conversion efficiency,  $\eta$ , (<7%), *a*-Si:H solar panels are represented primarily in niche markets, such as calculators, battery chargers etc. A potential application exists in the use of *a*-Si:H semi-transparent solar panels (Power Glass<sup>TM</sup>) for use in office buildings to replace tinted glass where the conventional opaque crystalline Si cannot compete. To address this market, we are in the process of developing *a*-Si:H panels on inexpensive plastic materials (IP) which lends itself to mass production via the use of our patented reel-to-reel cassette cluster tool approach [1,2,3]. Considerable work has been done on solar panels using expensive polyimide (e.g. Kapton) as the substrate, since its glass transition temperature,  $T_g$ , is  $\sim 250^\circ\text{C}$  or higher which is above the normal deposition temperature,  $T_s$  ( $\sim 230^\circ\text{C}$ ), of *a*-Si:H; however, as this type of substrate is expensive, the economics of the application demand a lower cost plastic substrate, such as PET, PES etc. which possess a much lower  $T_g$  than the polyimides. To this end, we have concentrated on developing *a*-Si:H based solar cells with  $T_s < 150^\circ\text{C}$ . In this paper, we report a monolithic series connected semi-transparent (transmission > 40%) *a*-Si:H solar cell panel (substrate area  $30 \times 40 \text{ cm}^2$ ), with an i-layer thickness < 2000 Å and an active area  $\eta \sim 3\%$ . We have successfully fabricated laser scribed series connected mini-modules (area up to  $20 \text{ cm}^2$ ) on glass and plastic substrates with an aperture area  $\eta > 3\%$ . In addition, we are currently building a reel-to-reel cassette cluster tool system with a web width of 30 cm to accommodate inexpensive plastic substrates which could be used to construct such semi-transparent panels.

### EXPERIMENTAL

*a*-Si:H films and solar cells/panels were produced in a commercially available PECVD cluster tool system specifically designed for the thin film semiconductor market and manufactured by MVSystems, Inc. The samples were prepared on a  $30 \times 40 \text{ cm}^2$  substrate carrier situated on the anode side of the RF electrode assembly. Deposition conditions were: RF power 20-60 Watt, an anode-cathode distance of 1-6 cm, flow rate of silane 2-30 sccm, flow rate of hydrogen 10-100 sccm, deposition pressure 100-700 mTorr, and  $T_s < 150^\circ\text{C}$ . The  $p^+$ -layer consisted of *a*-SiC:H:B and was deposited from  $\text{SiH}_4$ ,  $\text{CH}_4$  and  $\text{B}_2\text{H}_6$  gas mixtures, while the  $n^+$ -

layer was prepared using a SiH<sub>4</sub> and PH<sub>3</sub> gas mixture. ITO and ZnO materials were sputtered from InSnO<sub>2</sub> and Al doped ZnO targets, respectively. The opto-electronic properties of single a-Si layers were characterized by photo ( $\sigma_{ph}$ ) and dark ( $\sigma_D$ ) conductivity and the band gap  $E_g$  was determined using Tauc's plot.

## RESULTS AND DISCUSSION

As plastics are generally hygroscopic, out-gassing from the material can lead to oxygen and water in the vacuum chamber which then contaminate the *a*-Si:H films; hence prior to the deposition, the plastic substrates were cleaned and degassed in vacuum within the cluster tool for a specific period of time at an elevated temperature. In Table 1, we first consider the properties of n<sup>+</sup> and p<sup>+</sup> type layers when the deposition temperature,  $T_s$ , is lowered to below 150°C. Even though the n<sup>+</sup>-layer showed very similar electrical properties on glass and plastic

**Table 1.** Comparison of p<sup>+</sup> and n<sup>+</sup>-layer properties on glass and inexpensive plastic (IP) substrates.

Layer	Substrate	$\sigma_D$ (S/cm)	$\sigma_{ph}$ (S/cm)	$E_g$ (eV)
p <sup>+</sup>	Glass	$3.4 \cdot 10^{-6}$	$5.5 \cdot 10^{-6}$	2.03
	IP	$6.0 \cdot 10^{-7}$	$1.3 \cdot 10^{-6}$	1.93
n <sup>+</sup>	Glass	$8.7 \cdot 10^{-4}$	$1.3 \cdot 10^{-3}$	
	IP	$3.5 \cdot 10^{-4}$	$6.5 \cdot 10^{-4}$	

substrates, the dark conductivity,  $\sigma_D$ , of the n<sup>+</sup>-layer is lower ( $\sim$  factor 10) than usually obtained using a higher  $T_s \sim 230^\circ\text{C}$ . This aspect may introduce a barrier at the ITO/n<sup>+</sup> interface. In Table 2, we compare conventional, state-of-the-art *a*-Si:H intrinsic layers deposited at  $T_s \sim 230^\circ\text{C}$  on glass substrates with those deposited at  $T_s < 150^\circ\text{C}$  on IP substrates. As discussed elsewhere [2], an indicator of a low density of states, DOS, in the material is the value of  $\gamma$  derived from  $\ln \sigma_{ph} \propto \gamma \ln F$ , where  $F$  is the intensity of illumination and  $\sigma_{ph}$  is the photoconductivity. For instance, low DOS material generally exhibits a  $\gamma$  in excess of 0.9 in such a plot. As the DOS increases,  $\gamma$  decreases to a lower value. We note that with judicious use of the processing conditions for

**Table 2.** Comparison of the properties of *i*-layer deposited on glass ( $T_s \sim 230^\circ\text{C}$ ) and on inexpensive plastic (IP) substrate ( $T_s \sim 150^\circ\text{C}$ ).

Substrate	$\sigma_D$ (S/cm)	$\sigma_{ph}$ (S/cm)	$\gamma$	$E_g$ (eV)
Glass at $T_s \sim 230^\circ\text{C}$	$\sim 10^{-10}$	$> 10^{-5}$	0.95-1.00	$\sim 1.80$
IP at $T_s < 150^\circ\text{C}$	$3.2 \cdot 10^{-10}$	$2.2 \cdot 10^{-5}$	1.0	1.9

the *i*-layer for  $T_s < 150^\circ\text{C}$ , the properties of the material deposited on the IP substrate is virtually equivalent to the state-of-the-art properties obtained normally on a glass substrate at a higher  $T_s$ .

Fig. 1 shows the transmission as a function of wavelength of sputtered ITO and ZnO both deposited at room temperature. It should be noted that prior to the deposition, the IP had been degassed, as discussed above. Typical resistivities of ITO and ZnO were measured to be  $3.3 \times 10^{-4}$  and  $4.1 \times 10^{-4}$  ( $\Omega\text{cm}$ ) respectively.

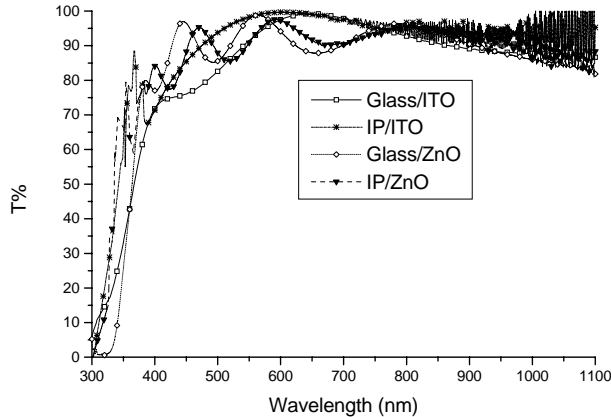


**Figure 1.** The transmissions of ITO and ZnO deposited on glass and IP type substrates.

## SEMI-TRANSPARENT SOLAR CELLS

Table 3 shows the performance of devices constructed, in the configuration p-i-n with  $T_s < 150^\circ\text{C}$ , simultaneously on three different types of substrates; (a) ITO coated glass, (b) ITO coated IP, and (c) TCO coated glass (TCO is defined as Asahi Type U, which is a textured  $\text{SnO}_2:\text{F}$  coated glass) with evaporated Ag back contacts. We note that irrespective of the substrate used, all the devices exhibited similar open circuit voltages  $V_{oc} \sim 0.85\text{V}$ . As is to be expected, the highest short circuit current density  $J_{sc}$  was obtained on the textured TCO substrate which can trap light more efficiently within the solar cell. Under blue light illumination, all the devices exhibited a fill factor  $FF > 0.7$  which is indicative of a good p/i junction formation. However all the devices showed a poor  $FF (< 0.6)$  under red and white illumination, which is indicative of an increased DOS within the i-layer; this aspect is reinforced since the devices had an increased diode quality factor,  $Q (> 1.8)$ , in comparison with the state-of-the-art value of  $\sim 1.6$ , which is normally obtained using  $T_s \sim 230^\circ\text{C}$ . This result appeared to conflict with the data shown in Table 2, where the i-layer, deposited at  $T_s < 150^\circ\text{C}$ , was shown to possess a low DOS. However, as we discussed previously, while we performed degassing of the IP prior to deposition, it is possible that the degassing procedure, in terms of time and temperature was insufficient thus leading to residual impurities within the chamber. As the devices for  $T_s < 150^\circ\text{C}$  on glass and IP in Table 3 were fabricated simultaneously, it is therefore possible that the i-layer may have become contaminated by  $\text{H}_2\text{O}$  vapor emanating from the IP during the deposition. Support for this can also be seen from Table 4, where performance of the devices on glass for  $T_s < 150^\circ\text{C}$ , but in the absence of IP in the chamber (device A), is compared with those devices in present of IP (devices B and C). We see that, without IP present,  $Q$  is indeed lower ( $\leq 1.7$ ), whereas the  $FF$  under red and white illumination have improved significantly from the data shown in Table 3. On the other hand, repeating the runs with the glass and IP together, designated as devices B and C, we see that once again  $Q$  has increased and the  $FF$  in the red and white have decreased significantly, which implies an increase in the DOS within the i-layer. It is

therefore evident that we need to develop better out-gassing procedures to avoid contamination of the i-layer.

**Table 3.** Comparison of p-i-n devices using different substrates and bottom contacts, with  $T_s < 150^\circ\text{C}$ , for an i-layer thickness of  $4000\text{\AA}$ .

	Glass/TCO/pin/Ag	Glass/ITO/pin/Ag	IP/ITO/pin/Ag
$V_{oc}$ (V)	0.86	0.86	0.85
$J_{sc}$ ( $\text{mA}/\text{cm}^2$ )	9.6	7.5	5.4
FF (white)	0.57	0.54	0.55
FF (blue)	0.70	0.73	0.70
FF (red)	0.58	0.52	0.55
Q Factor	1.9	1.8	1.9

**Table 4.** Comparison of pin devices with/without IP process for  $T_s < 150^\circ\text{C}$  for a layer thickness of  $\sim 2000\text{\AA}$ .

	A Glass without IP	B Glass With IP	C IP
$V_{oc}$ (V)	0.86	0.84	0.83
$J_{sc}$ ( $\text{mA}/\text{cm}^2$ )	6.1	6.0	5.8
FF (white)	0.65	0.52	0.53
FF (blue)	0.71	0.74	0.73
FF (red)	0.69	0.49	0.52
Q Factor	$\leq 1.7$	1.9	1.9

As discussed above, the application under consideration involves transparency of the solar panel. Fig. 2 shows the relationship between the film transmission and *i*-layer thickness for a structure type IP/ITO/pin/ITO. Note that transmission is in excess of 40% for a thickness of  $\sim 2000\text{\AA}$  at a wavelength of 600nm.

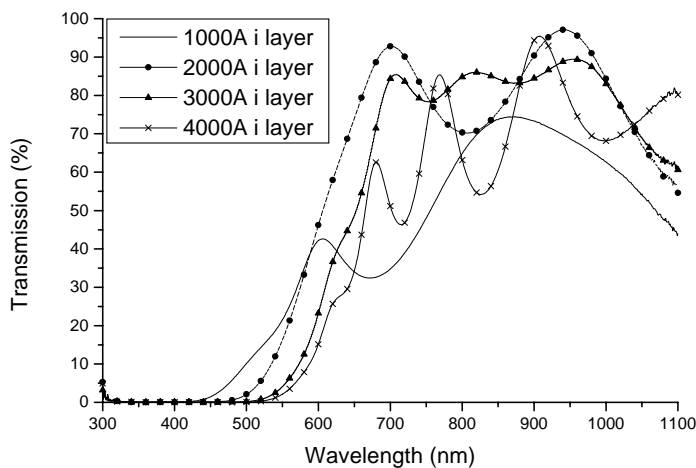


**Figure 2.** Transmission  $T(\lambda)$  of IP/ITO/pin/ITO structures with different *i*-layer thicknesses.

## SEMI-TRANSPARENT MODULES ON GLASS AND PLASTIC USING MECHANICAL MASKS AND LASER SCRIBING TECHNIQUES.

We have constructed a series connected semi-transparent module on an IP substrate (substrate area  $30 \times 40 \text{ cm}^2$ ), as shown in Fig. 3(a), which has yielded  $J_{sc} \sim 5 \text{ mA/cm}^2$ ,  $V_{oc} > 10 \text{ V}$ , and an active area efficiency  $\eta$  of  $\sim 2.7\text{-}3\%$ . Since these modules were made using mechanical masks, the area loss is large. With laser scribing technique, this loss can be minimized to about 5%. Fig. 3(b) shows an all laser cut series connected mini-module and constructed in the configuration glass/ITO/pin/ITO.

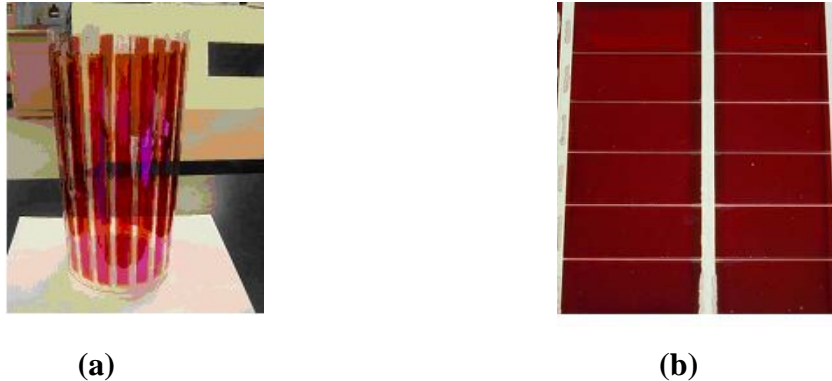


**Figure 3.** (a) Monolithic series connected panel on IP (mechanically masked, substrate area:  $30 \times 40 \text{ cm}^2$ ); and (b) A laser scribed series connected panel on glass substrate (area:  $6 \times 8.4 \text{ cm}^2$ ).

Compared with rigid glass substrates, plastic has a much lower melting point, at which temperature it starts to deform. As a result, conventional laser scribing processes often lead to damage of the IP substrate due to absorption of excessive laser power by the IP. Fig. 4(a) shows an image of a laser cut on ITO directly deposited on the IP. Note that the white rings surrounding the cut are due to deformation of the IP. With the insertion of a passivation layer between ITO (or ZnO) and the IP, the laser power required to separate ITO (or ZnO) can be reduced, resulting

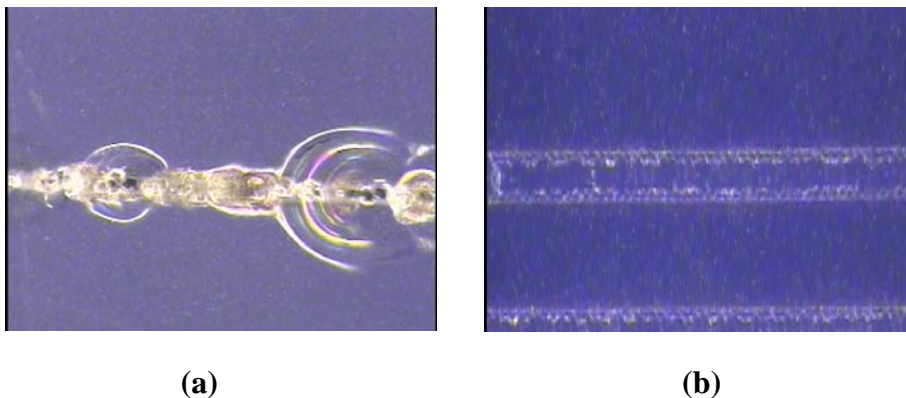


**Figure 4.** (a) A laser cut ITO line on IP and (b) with a passivation layer deposited in between ITO and IP. The laser cut is  $\sim 20 \text{ }\mu\text{m}$  wide.

in less damage to the IP. By optimizing laser scribing parameters (e.g. power, scribing speed and repetition frequency, etc), separation of the ITO without damage on IP can be achieved, as shown in Fig. 4(b).

For a monolithic integration of a module on plastic involving IP/ITO/pin/ITO, three laser cuts are necessary as shown in Fig. 5. As laser scribing can damage the individual layers and create extra shunt paths, either due to debris left after each cut or crystallization of the a-Si pin

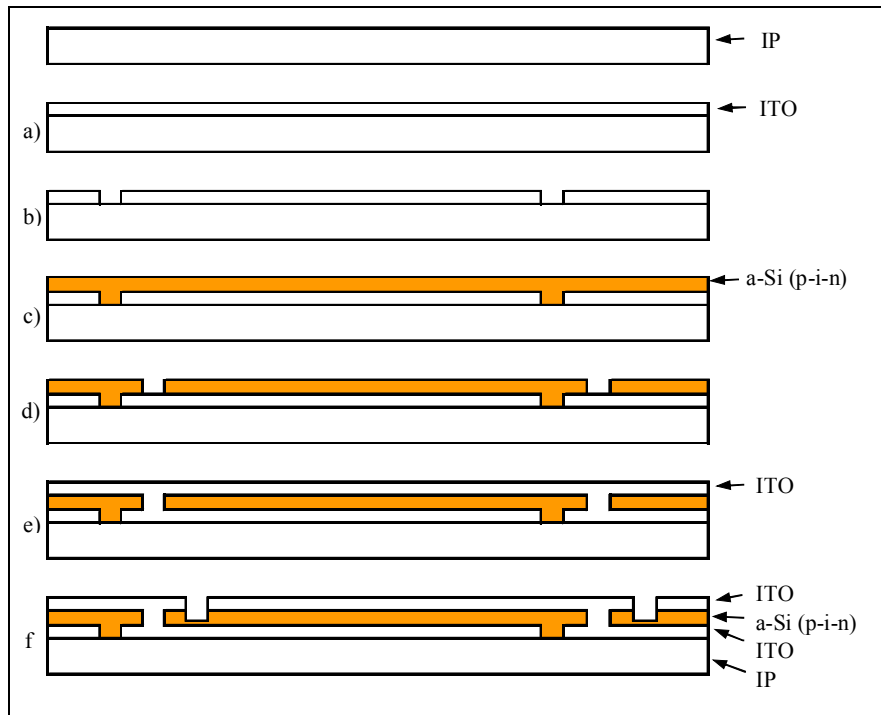


**Fig. 5.** Step-by-step schematic for monolithic integration of a-Si panels. Steps b, d and f show the laser cuts.

layers, it is instructive to ensure that the performance of the diagnostic cells (small area and no laser scribing) correspond well with the performance of the laser scribed panels. In this context we have deposited several types of diagnostic cells on glass and IP simultaneously, as shown in Fig. 6 and 7.

- Fig. 6a shows the configuration of glass /TCO /pin/ silver contact- diagnostic cells of area  $0.25 \text{ cm}^2$ ,
- Fig. 6b shows glass/ITO (specular)/pin/Ag- diagnostic cells of area  $0.25 \text{ cm}^2$ ,
- Fig. 7a shows the data for IP/ITO/pin/ITO- diagnostic cells of area  $0.25 \text{ cm}^2$ ,
- Fig. 7b shows the data for laser scribed mini-modules, series connected, of area up to  $20 \text{ cm}^2$ .

We note that as the i-layer is decreased in thickness, the FF increases quite considerably from  $\sim 0.56$  to  $\sim 0.67$  for  $4000\text{\AA}$  and  $2000\text{\AA}$  thicknesses respectively. It should be noted that this data is consistent with the data displayed in Table 3. The current density in the textured TCO

sample (Fig. 6a), as is to be expected, is considerably higher than in the diagnostic samples using specular ITO (Fig. 6b).

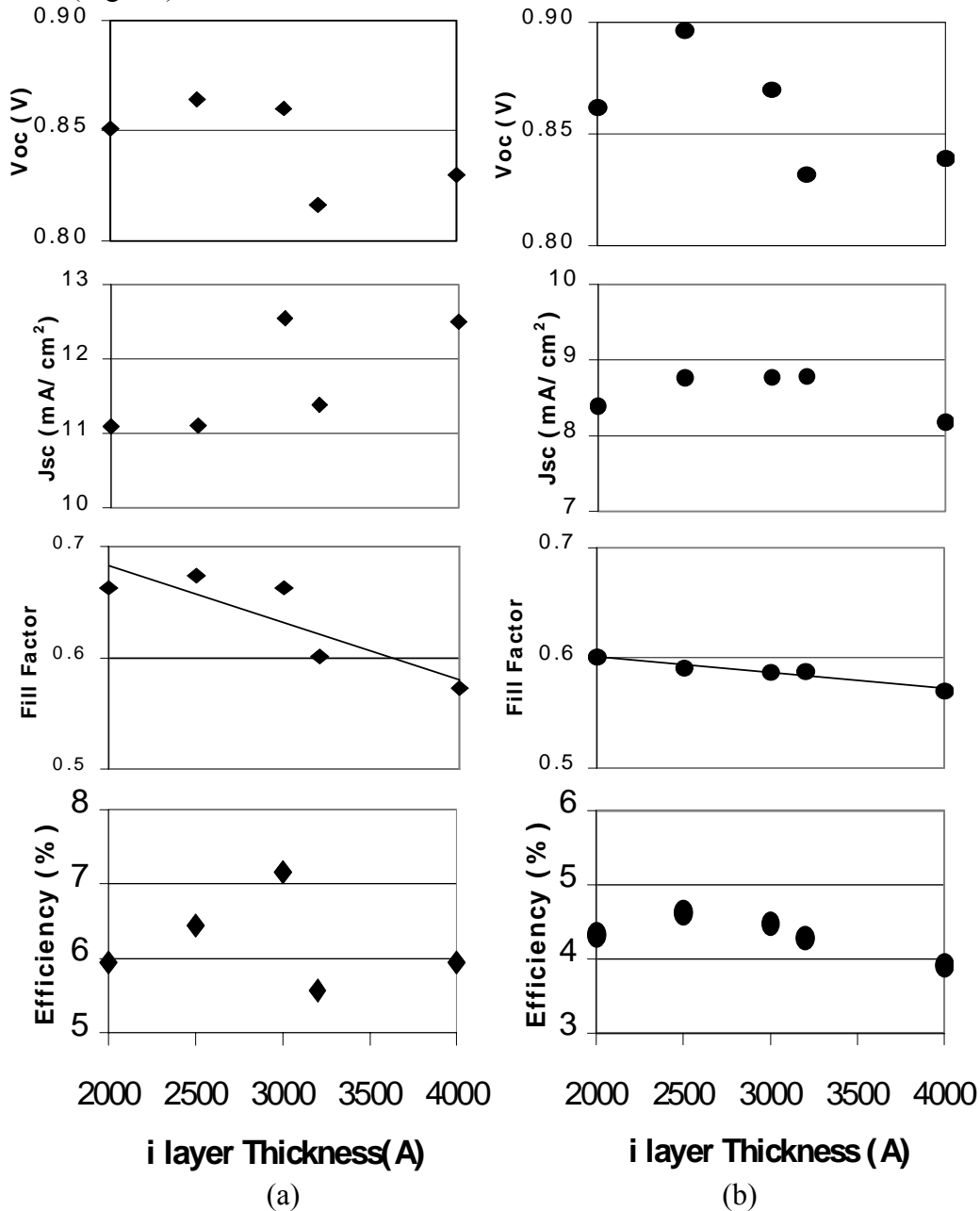


**Figure 6:** AM1.5 cell characteristics as a function of I-layer thickness for (a) glass/TCO/pin/Ag control cells, (b) glass/ITO/pin/Ag control cells, (TCO is defined as textured Asahi type U-SnO<sub>2</sub>).

Fig. 7a shows the results of diagnostic cells on IP and we note that their current density is slightly lower than on glass/ITO samples of Fig. 6b. Some of this reduction can be explained by reflection losses which are larger for air/IP interface (11%) versus glass (4%). However we note that the FF for both types of samples are ~0.6 for a thickness of 2000Å. Fig. 7b shows laser scribed mini-modules with 5 cells connected in series with a total area up to 20 cm<sup>2</sup>. The FF of laser scribed mini-module is reduced to approx 0.55 and is slightly lower than in the

corresponding diagnostic cell shown in Fig. 7a. The loss may be attributed to a slight series resistance emanating from the ITO layer itself. The apparent maximum in the efficiency at about 2500Å is likely to be an artifact, as the Voc in these samples was reduced for samples for 2000Å i-layer thickness. We note that this did not occur in the samples prepared on TCO and ITO coated glass of Fig.'s 6a and 6b. The apparent reduction in the Voc on IP substrates is likely to be due to some non-uniformity in thickness that may have occurred during the p-layer deposition.

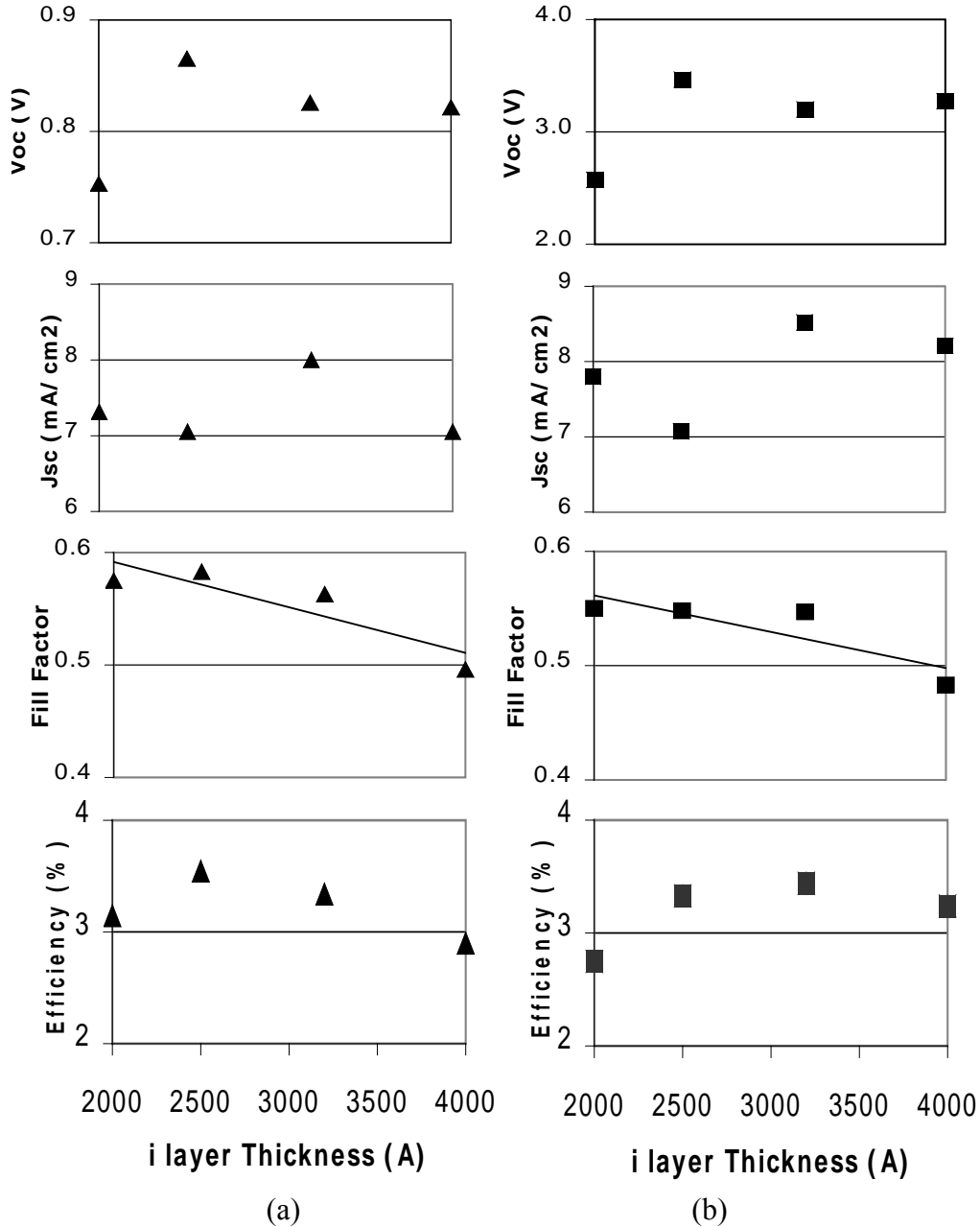


**Figure 7.** AM1.5 cell characteristics as a function of i-layer thickness in configuration, (a) IP/ITO/pin/ITO diagnostic cells and (b) series-connected, laser-scribed mini-modules-IP/ITO/pin/ITO.

## IMPROVEMENT IN EFFICIENCY

By increasing the optical bandgap of the i-layer, the Voc of devices increases notably to  $\sim 0.96$  V, as shown in Table 5. This has substantially increased the conversion efficiency of the semi-transparent solar cell. It should be noted that the FF $\sim 0.77$  under blue light illumination, indicating an excellent p/i interface, and FF under red light illumination is  $\sim 0.7$ , implying a low density of states in the bulk. However, FF under white light illumination (high flux intensity) is lowered to  $\sim 0.6$ , implying that there is a resistive problem which could be either associated with the ZnO front contact or the p/ZnO interface. Solution of this issue and retention of the FF  $\sim 0.7$  would indeed lead to a device with  $\eta \sim 6.0\%$ . With an ITO back contact, the device efficiency could be  $\sim 5.0\%$  and the transmission in excess of 25% at a wavelength of 600 nm.

**Table 5.** Solar cells in configuration ZnO/pin/Ag.

i-layer thickness (Å)	Voc (V)	Jsc (mA/cm <sup>2</sup> )	FF (AM 1.5)	FF (blue light)	FF (red light)	$\eta$ (%)
2000	0.93	7.5	0.63	0.77	0.68	4.39
2000	0.96	8.5	0.6	0.77	0.69	4.90
2000	0.93	8.5	0.66	0.77	0.74	4.94

## REEL-TO-REEL CASSETTE CLUSTER TOOL APPROACH

In conventional roll-to-roll systems using flexible substrates for solar cell manufacture, the material passes through the various deposition zones in one sequence. As these zones cannot be physically separated, there is an inevitable cross contamination leading to poorer device performance, although an attempt is made to minimize it, via the use of slits and gas curtains between the deposition zones [3]. To overcome the severe drawback of this approach, MVS's patented reel-to-reel cluster tool [1] involves the use of a cassette, which houses a flexible material, as shown in Fig. 8. Each process chamber contains appropriate drives and mechanisms

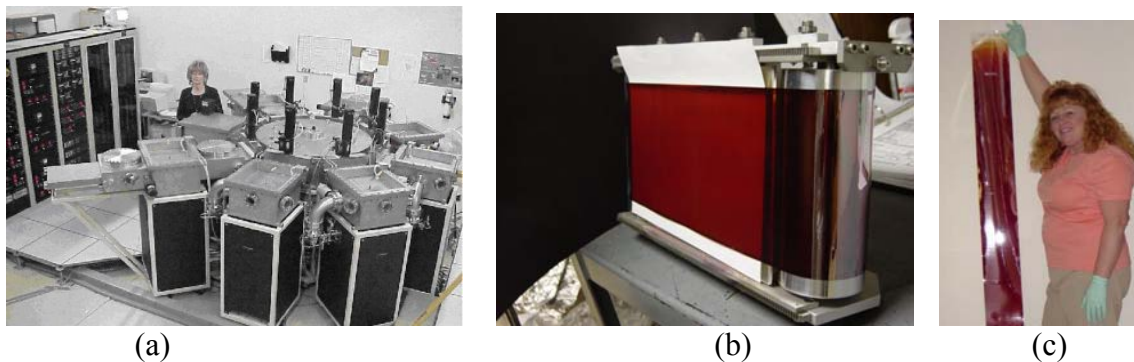


**Figure 8.** (a) Cluster tool consisting of numerous PECVD and sputter chambers. This can accommodate rigid and flexible substrates housed in reel-to-reel cassette, as shown in (b). (c) shows a uniform a-Si film on a 15cm web.

to locate the cassette over a deposition zone (e.g. PECVD or sputtering). Within the process chamber, the cassette is engaged for movement of the flexible material from one reel to another

during the deposition process. At the end of deposition, the flexible material is returned to its original reel and locked into position and disengaged from the chamber for transport; the entire cassette is then transported to the next chamber in a similar fashion to that for a rigid substrate (i.e., using a robotic arm). Hence cross contamination is eliminated for fabrication on flexible substrates. We have recently shipped a system with web width of 15 cm and are building a larger system with web width of 30 cm.

## CONCLUSION

We have developed a monolithic series connected semi-transparent (transmission > 40%) *a*-Si:H module (substrate area 30 × 40 cm<sup>2</sup>), with an i-layer thickness < 2000 Å and an active area efficiency  $\eta \sim 3\%$ . We have also developed all laser scribed semi-transparent mini-modules with an aperture area  $\eta > 3\%$ . This could, together with the use of reel-to-reel cassette cluster tool system for mass production, result in a competitive product in the market of Building Integrated Photovoltaics.

## ACKNOWLEDGEMENTS

We should like to thank XsunX Inc. for partially funding this project and E.Valentich for his assistance in processing solar cells and modules.

## REFERENCES

1. A. Madan, "Semiconductor Vacuum Deposition System and Method having a Reel to Reel Substrate Cassette", US patent #6,258,408B1. MRS Proc. 814, (2004), I2.9/A3.9.
2. X. Zhang, M. Saemann, J. Hu, A. Kunrath, A. Berger, and A. Madan, Proceedings of the IEEE 4<sup>th</sup> World Conference on Photovoltaic Energy Conversion, Hawaii (2006).
3. X. Zhang, J. Hu, A. Kunrath, I. Matulionis, R. Ahrenkiel, and A. Madan, Proceedings of the 21<sup>st</sup> European Photovoltaic Solar Energy Conference, Dresden (2006).
4. T.J. McMahon and A. Madan, Appl. Phys. Lett. **57**, 5302, (1985).
5. G. Demaggio, J. Doehler, T. Ellison, M. Izu, S. Jones, J. Karn, R. Kopf, M. Lycette, W. Messing, H. Ovshinsky, S. Ovshinsky, A. Banerjee, J. Call, W. Chan, G. Dio, S. Guha, K. Hoffman, R. Liu, P. Nam, J. Yang, NCPV and Solar Program Review Meeting, March 24-26, 2003, Denver, CO, NREL-CD-520-33586.